Atomically Thin $CrCl_3$: An in-Plane Layered Antiferromagnetic Insulator

Xinghan Cai,[1,2] Tiancheng Song,[1] Nathan P. Wilson, [1] Genevieve Clark,[3] Minhao He,[1] Xiaoou Zhang,[4] Takashi Taniguchi,[5] Kenji Watanabe,[5] Wang Yao,[6] Di Xiao,[4] Michael A. McGuire,[7] David H. Cobden,[1] Xiaodong Xu[1,3]*

[1]Department of Physics, University of Washington, Seattle, Washington 98195, USA.
[2]National Key Laboratory of Science and Technology on Micro/Nano Fabrication, Department of Micro/Nano Electronics, Shanghai Jiao Tong University, Shanghai 200240, China.
[3]Department of Materials Science and Engineering, University of Washington, Seattle, Washington 98195, USA.
[4]Department of Physics, Carnegie Mellon University, Pittsburgh, Pennsylvania 15213, USA.
[5]National Institute for Materials Science, Tsukuba, Ibaraki 305-0044, Japan.
[6]Department of Physics and Center of Theoretical and Computational Physics, University of Hong Kong, Hong Kong, China.
[7]Materials Science and Technology Division, Oak Ridge National Laboratory, Oak Ridge, Tennessee 37831, USA.

*Correspondence to: xuxd@uw.edu

Abstract: The recent discovery of magnetism in atomically thin layers of van der Waals (vdW) crystals has created new opportunities for exploring magnetic phenomena in the two-dimensional (2D) limit. In most 2D magnets studied to date the c-axis is an easy axis, so that at zero applied field the polarization of each layer is perpendicular to the plane. Here, we demonstrate that atomically thin $CrCl_3$ is a layered antiferromagnetic insulator with an easy-plane normal to the c-axis, that is the polarization is in the plane of each layer and has no preferred direction within it. Ligand field photoluminescence at 870 nm is observed down to the monolayer limit, demonstrating its insulating properties. We investigate the in-plane magnetic order using tunneling magnetoresistance in graphene/$CrCl_3$/graphene tunnel junctions, establishing that the interlayer coupling is antiferromagnetic down to the bilayer. From the temperature dependence of the magnetoresistance we obtain an effective magnetic phase diagram for the bilayer. Our result shows that $CrCl_3$ should be useful for studying the physics of 2D phase transitions and for making new kinds of vdW spintronic devices.

Keywords: 2D magnetic insulator, in-plane layered antiferromagnetism, magnetic tunnel junction, weak magnetic anisotropy, magnetic phase transition

The experimental observation of magnetism in atomically thin films[1-8] has opened a new avenue to study novel magnetic multilayered devices using 2D materials[9-21]. To date, all magnetic compounds that have been successfully synthesized down to the monolayer limit exhibit strong Ising anisotropy, which supports an out-of-plane magnetization within each layer. In this regard,

$CrCl_3$ represents a curious case in that bulk $CrCl_3$ is known to be a weakly coupled, layered antiferromagnet with small XY anisotropy (Figure 1a)[22-25]. Therefore, exfoliating $CrCl_3$ offers the intriguing possibility to realize a strictly 2D magnetic insulator with in-plane magnetization. This could be useful for investigating how a magnet with weak anisotropy evolves on approaching the 2D limit. The monolayer may behave as a good approximation to the 2D XY-model, analogous to thin film superfluids, superconductors and liquid crystals[26,27], allowing the study of the Berezinskii–Kosterlitz–Thouless (BKT) transition[28] and related phenomena. Moreover, the in-plane magnetization is also complementary to the out-of-plane magnetization in terms of the proximity effect[29-33] when $CrCl_3$ is layered with other 2D materials.

$CrCl_3$ flakes were exfoliated onto SiO_2/Si substrates. In atomic force microscope images (Figure 1b), bilayers and trilayer regions appear 1.2 nm and 1.8 nm thick, respectively, consistent with a previous report[25]. Figure 1c shows both the circular polarization components of the photoluminescence (PL) from a ~ 5 nm thick sample at a temperature of 2 K, well below the Neel temperature of ~ 14 K. The excitation laser is 20 μW, linearly polarized, and at 532 nm. A single broad peak centered at ~ 870 nm is seen, analogous to the parity-forbidden *d-d* ligand-field transition in CrI_3[34]. Unlike in CrI_3, where the out-of-plane magnetization component results in spontaneously circularly-polarized PL, the two polarization components in thin bulk $CrCl_3$ are indistinguishable, consistent with the in-plane magnetization determined in its bulk crystal. This PL emission feature persists down to the monolayer $CrCl_3$ (Figure 1d), implying that the insulating nature retains in $CrCl_3$ to its 2D limit.

To investigate the in-plane magnetization we employ vertical tunneling measurements, which are sensitive to the relative alignment of spins in different layers. As sketched in Figure 2a, a few layer $CrCl_3$ tunnel barrier is sandwiched between top and bottom thin graphite flakes to form magnetic tunnel junction (MTJ), this being further encapsulated in hexagonal boron nitride (h-BN) to avoid degradation (see Methods). The tunneling junction area is typically less than ~1 μm^2 to avoid effects caused by lateral magnetic domain structures[1,13]. Figure 2b shows the tunneling current, I_t, as a function of DC bias voltage, V, measured at 2 K for a bilayer $CrCl_3$ device whose optical image is inset. With an applied in-plane magnetic field $\mu_0 H_{in}$=2 T (red trace) the current is enhanced relative to its value at zero field (blue trace), implying a change in the spin configuration of the $CrCl_3$[35]. The bottom inset shows the tunneling magnetoresistance (TMR), defined as $100\% \times [I_t(2\ \mathrm{T}) - I_t(0)]/I_t(0)$[13]. The TMR is largest at low bias, where the response is linear. Figure 2c shows the tunneling current, I_t, here measured using a small AC bias of V_{ac} = 1 mV, as a function of magnetic field. For either in-plane field (H_{in}, orange) or out-of-plane field (H_{out}, green), I_t increases smoothly before plateauing out when the field exceeds a critical value ($\mu_0 H_{in}^c$ = 1.2 T and $\mu_0 H_{out}^c$ = 1.5 T). This behavior is similar to that seen for an in-plane field in CrI_3 MTJs. It implies that the spin polarizations of the two layers are opposite at zero field, suppressing the tunneling current by a spin-filtering effect, but become increasingly aligned due to the Zeeman term in an external field. This in turn suggests that the layered antiferromagnetic order of the bulk crystal, with in-plane ferromagnetic polarization that alternates in direction between adjacent layers, persists in the bilayer limit.

The fact that H_{out}^{c} is only slightly larger than H_{in}^{c}, and the smooth rise of I_t seen for both field orientations, are consistent with relatively weak anisotropy in the material. Indeed, the field dependence of the tunneling current can be well fit by a simple model of two antiferromagnetically coupled macrospins with easy-plane anisotropy,

$$H = J_{AF}\boldsymbol{s}_1 \cdot \boldsymbol{s}_2 + \frac{K}{2}\left(s_{1,z}^2 + s_{2,z}^2\right) - g\mu_B \boldsymbol{B} \cdot (\boldsymbol{s}_1 + \boldsymbol{s}_2),$$

where $J_{AF} > 0$ is the interlayer antiferromagnetic exchange, $K > 0$ is the easy-plane anisotropy energy, and $\boldsymbol{B}$ is the magnetic field. According to our fitting, the anisotropy is $KS/g\mu_B = 0.27$ T and interlayer coupling is $J_{AF}S/g\mu_B = 0.6$ T (See Supplementary material). We note that there is some asymmetry of I_t as a function of H_{in}, associated with hysteresis as shown in Figure 2d. This might be due to a spin-flop transition associated with a previously reported, very small easy-axis anisotropy (10 Oe) within the easy-plane[24,25]. No hysteresis is seen as a function of H_{out} (Figure 2d, inset), as expected for spin canting in a magnetic field perpendicular to the zero-field polarization. This is in sharp contrast to the situation in bilayer CrI_3, where the transition from antiferromagnetic to a fully aligned ferromagnetic state in a perpendicular field is a sudden spin-flip transition.

The picture of layered antiferromagnetism is further supported by measurements on a trilayer $CrCl_3$ MTJ device (Figure 3), an optical micrograph of which is inset to Figure 3b. The thicker barrier presented by a trilayer leads to much weaker tunneling which necessitates a much larger bias voltage to achieve a suitable signal to noise ratio. Without loss of generality, a DC bias of 600 mV is applied (See supplementary material for the bias voltage dependent tunneling measurements). As seen in Figure 3a, I_t increases smoothly with H_{out}, again consistent with gradual spin canting out of the layers as in the bilayer case[13]. However, as a function of H_{in} the current exhibits a plateau near zero field below a critical value, above which it smoothly rises and reaches a plateau when the magnetic field is large enough to align all three layers to the fully spin polarized state.

To test for magnetic anisotropy within the plane of the layers, we measured the tunneling current while varying the orientation, θ, of H_{in} within the plane. Figure 3b shows I_t as a function of H_{in} at selected angles, while Figure 3c is a polar plot of I_t as a function of angle at selected magnetic fields. No significant dependence on θ is observed, implying that the overall magnetic order can rotate freely about the c-axis, i.e., the plane of the layers is an easy plane. The observed plateau of tunneling current as a function of in-plane magnetic field is due to the uncompensated total magnetization in a trilayer, consistent with the picture of layered antiferromagnetism. We conclude that atomically thin $CrCl_3$ can be well described as a layered antiferromagnetic insulator with easy-plane magnetic anisotropy.

Figure 4a shows the tunneling current I_t measured AC with $V_{ac} = 5$ mV as a function of T at selected in-plane magnetic fields. At $H_{in} = 0$, on increasing T from base, at first I_t increases. This can be explained by suppression of the spin filtering effect due to thermal fluctuations which reduce the degree of antiferromagnetic alignment between the layers. Then, above a peak at the intralayer ferromagnetic critical temperature $T \sim 17$ K, I_t starts to decrease. This suggests that ferromagnetic

order within each layer assists coherent tunneling, and rising temperature suppresses this order. At still higher temperatures I_t increases again, as expected since once no magnetic order remains the tunneling rate should simply be activated. When an in-plane field is applied it competes with the antiferromagnetic alignment and reduces the temperature at which the AFM order appears, so the peak moves to lower T. It also increases net spin alignment above the critical temperature and so increases the current. For $\mu_0 H_{in} > 1.2$ T, the antiferromagnetism is completely suppressed and the spins are fully polarized at base temperature.

The results in Figure 4a can be presented in a more visualized way: dI_t/dT has been plotted as a function of the temperature at selected $\mu_0 H_{in}$ (Figure 4b). In the top panel, dI_t/dT clearly exhibits two times of the sign flip as T increases. This is similar to what has been reported in $CrCl_3$ 3D bulk crystal[25], which is interpreted as a two-step phase transition, i.e. from the layered antiferromagnetic phase to the ferromagnetic phase (first transition) and eventually to the paramagnetic phase (second transition) as T increases. Here we assign the peak (directed by the green arrow) in each curve to the critical temperature of the first transition and the dip (directed by the blue arrow) to the second one. For magnetic fields higher than 1.2 T, as shown in the bottom panel, no local maximum shows up, thus only T_c for the second transition is determined. In Figure 4c, we present the 2D semi-log plot of the normalized dI_t/dT as a function of both $\mu_0 H_{in}$ and T (see supplementary material for the plot without the normalization of dI_t/dT). This plot, though not a legitimate phase diagram, facilities comparison with the phase diagram of the 3D bulk crystal in which distinct transitions are identified between the layered AFM phase, a fully spin-polarized phase, and paramagnetic phase[25].

To recap, we find that the van der Waals magnetic insulator $CrCl_3$ shows layered antiferromagnetism down to the bilayer limit with the magnetic moments in the plane of the layers and little or no anisotropy within the plane. $CrCl_3$ thus provides a new model system for studying 2D in-plane magnetism and its proximate coupling to other 2D materials, such as 2D superconductors, topological insulators, and stacked heterostructures[30,36] for potential use in novel magneto-electronic devices[13-18].

During the final preparation of the manuscript, we became aware of the two relevant works posted on ArXiv[37,38].

METHODS

Device fabrication: V/Au (4 nm/40 nm) metal electrodes were deposited on a 90 nm SiO_2/Si substrate in the vicinity of the exfoliated h-BN thin flake (bottom h-BN), following the standard e-beam lithography procedures. Bulk $CrCl_3$ crystals were grown by chemical vapour transport, as described in detail in ref[25]. Few layer $CrCl_3$, cleaved from these crystals in an inert gas glovebox with oxygen and water levels below 1 ppm, was stacked between the pre-exfoliated top h-BN/graphite and bottom graphite and transferred onto the bottom h-BN using a polymer-based dry transfer technique[39]. Top/bottom graphite flakes were contacted by the pre-patterned metal electrodes and the tunnel junction was then fully encapsulated before finally dissolving the polymer in chloroform outside the glovebox. The thickness of the h-BN (5-35 nm) and graphite

(2-8 nm) were determined by atomic force microscopy, while the number of layers of $CrCl_3$ was identified from the optical contrast.

Optical measurements: Low-temperature magneto-PL measurements were performed in a closed-cycle cryostat with a superconducting magnet with field normal to the sample. The sample was excited by a continuous-wave laser (633 nm or 532 nm) with the power below 50 μW to avoid sample heating and degradation. The PL signal was detected by a silicon CCD array and the excitation and detection polarization were controlled using linear polarizers and half- and quarter-wave plates.

Electrical measurements: All magneto-transport measurements were carried out in a PPMS DynaCool cryostat (Quantum Design, Inc) with a base temperature of 1.8 K and magnetic field up to 9 T. The $CrCl_3$ MTJ devices were mounted in a Horizontal Rotator probe using either a Rotator Universal Sample Board (P103C), which allows rotations about an axis in the sample plane perpendicular to the magnetic field, or a Rotator Field Parallel Sample Board (P103D) for rotation about the magnetic field axis. The bias voltage is applied to the top graphite contact while the current from the bottom graphite contact is measured using a virtual-earth current preamplifier (DL Instruments; Model 1211). AC measurements were made using a lock-in amplifier (Stanford Research 830) at 13.7 Hz.

Figure Captions:

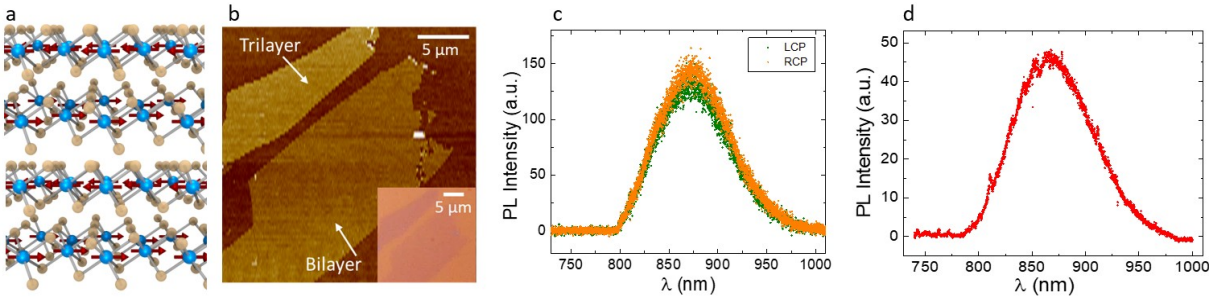

Figure 1. $CrCl_3$ crystal structure and the optical characterization. (a) Side view of the structure of $CrCl_3$. The colored balls represent Cr (blue) and Cl (grey), respectively. Red arrows indicate the magnetization. (b) Atomic force micrograph of few layer $CrCl_3$ flakes. The inset is an optical micrograph of the same area. (c) Left and right circular polarization components of photoluminescence from a 5 nm thick flake under a linearly polarized excitation at 532 nm. (d) Photoluminescence spectrum of a monolayer $CrCl_3$.

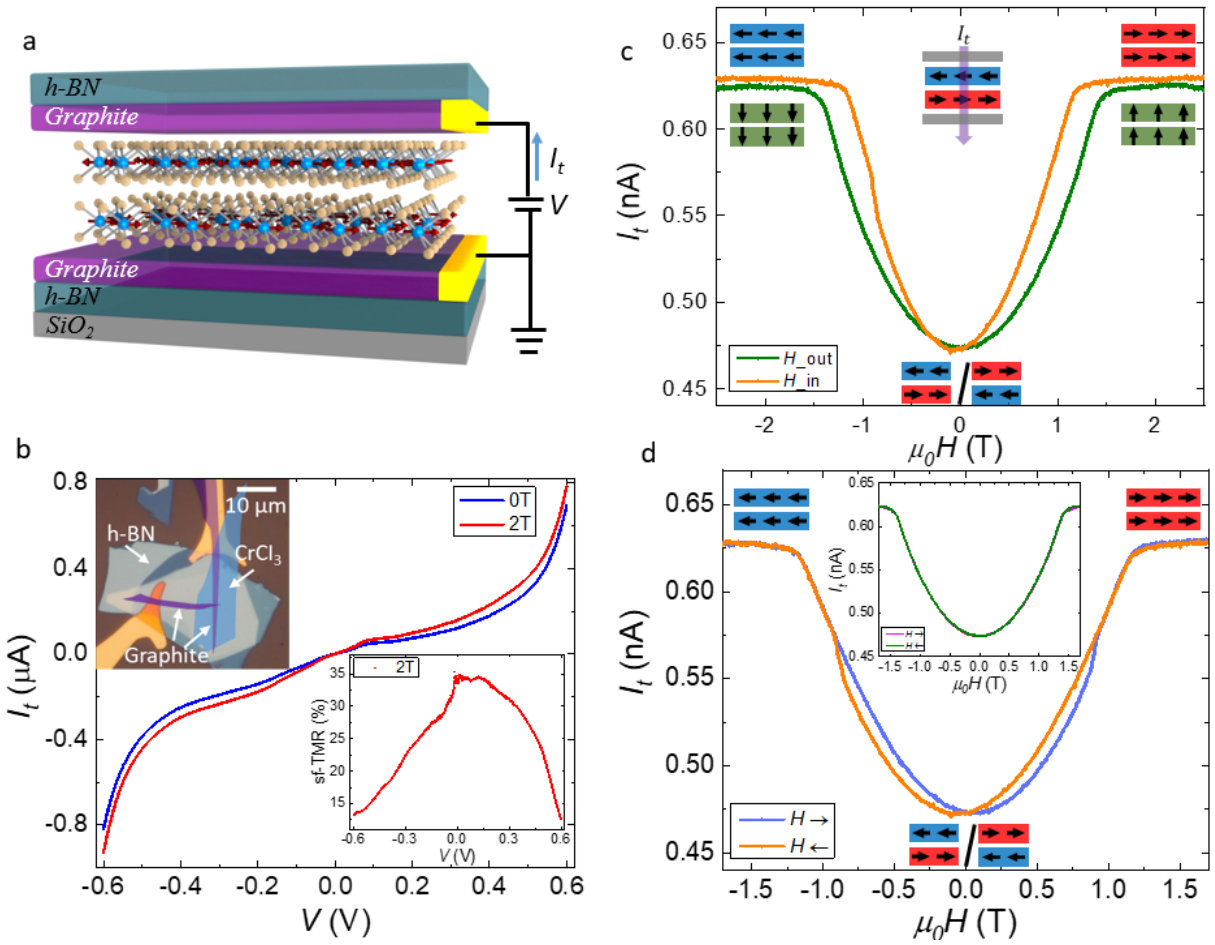

Figure 2. Magnetic field dependent tunneling in a bilayer $CrCl_3$ spin-filter magnetic tunnel junction (sf-MTJ). (a) Schematic of device with graphite contacts encapsulated by h-BN. (b) Tunneling current as a function of the DC bias voltage with (red) and without (blue) an in-plane magnetic field $\mu_0 H_{in}$=2 T. Top inset: optical microscope image of the device with false coloring for clarity. Bottom inset: TMR ratio. (c) Tunneling current I_t as a function of in-plane (orange) and out-of-plane (green) magnetic field for bias V_{ac} = 1 mV. The corresponding magnetic states are indicated. (d) Tunneling current vs in-plane magnetic field sweep in both directions. The magnetic configurations are indicated. Top inset: Tunneling current vs out-of-plane field swept in both directions, showing no hysteresis.

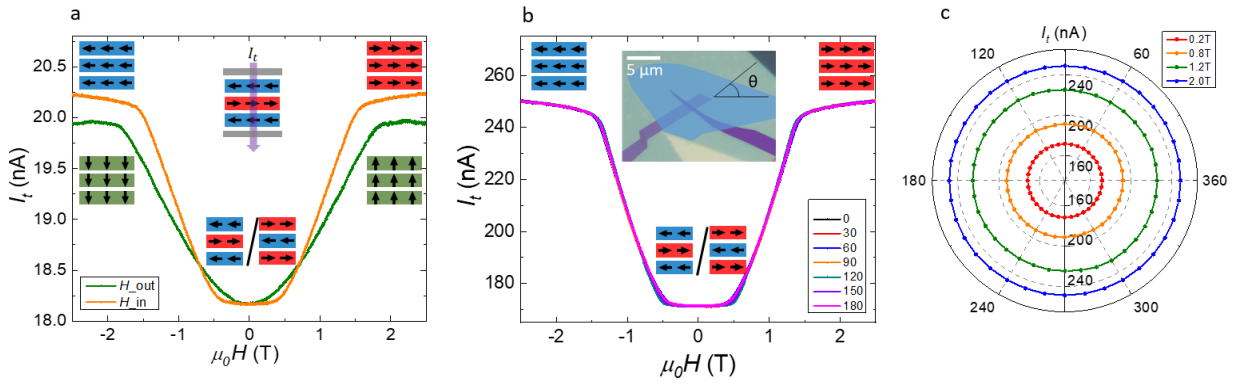

Figure 3. Magnetic field dependent tunneling in a tri-layer $CrCl_3$ sf-MTJ device. (a) Tunneling current I_t as a function of the in-plane (orange) and out-of-plane (green) magnetic field at V_{dc} = 600 mV. The corresponding magnetic states are indicated. (b) Tunneling current as a function of in-plane magnetic field at selected orientations θ (here V_{dc} = 750 mV). The inset is a false-color optical micrograph of the device with θ defined. (c) Polar plot of the tunneling current as a function of θ at selected magnetic fields.

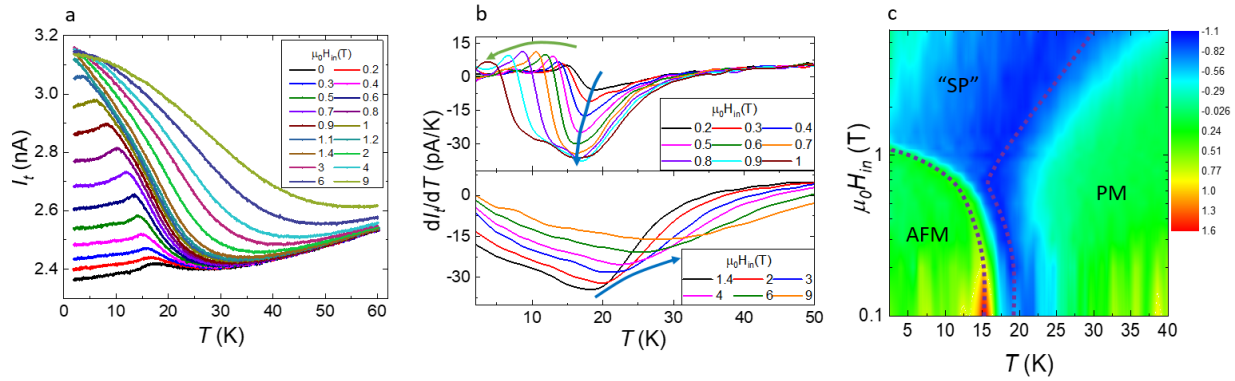

Figure 4. Temperature dependent tunneling and the magnetic phase diagram of bilayer $CrCl_3$. (a) Tunneling current I_t as a function of the temperature at selected in-plane magnetic fields with the AC bias voltage V_{ac} = 5 mV. (b) The derivative of the tunneling current to the temperature at low (top panel) and high (bottom panel) in-plane magnetic fields. The green/blue arrows indicate the critical temperature of the transition from layered antiferromagnetic/spin polarized to spin polarized/paramagnetic states, respectively. (c) Color plot of normalized dI_t/dT as a function of in-plane magnetic field H_{in} and temperature T. AFM: Layered antiferromagnetic. PM: Paramagnetic. SP: Fully spin polarized.

Acknowledgments: Funding: The work at UW is mainly supported by NSF MRSEC 1719797. Device fabrication and transport measurements are partially supported by NSF-DMR-1708419. Photoluminescence measurement is supported by DOE BES DE-SC0012509. Work at HKU is supported by the Croucher Foundation (Croucher Innovation Award), RGC of HKSAR (17303518P). Work at ORNL (M.A.M.) was supported by the US Department of Energy, Office of Science, Basic Energy Sciences, Materials Sciences and Engineering Division. K.W. and T.T. acknowledge support from the Elemental Strategy Initiative conducted by the MEXT, Japan, A3 Foresight by JSPS and the CREST(JPMJCR15F3), JST. D.X. acknowledges the support of a Cottrell Scholar Award. X.X. acknowledges the support from the State of Washington funded Clean Energy Institute and from the Boeing Distinguished Professorship in Physics.

Author Contributions: X.X., X.C., M.A.M. conceived the project. X.C. fabricated the devices, performed the experiments, and analyzed the data, assisted by T.S. and M.H. N.P.W. and G.C. performed photoluminescence measurements. X.Z. analyzed the macrospin model and the tunneling current dependence on the magnetic structure. X.X., D.X., W.Y., and D.H.C. supervised the project. M.A.M. provided and characterized bulk $CrCl_3$ crystals. T.T. and K.W. provided and characterized bulk hBN crystals. X.C., X.X., D.H.C. and D.X. wrote the manuscript with input from all authors.

Competing Financial Interests: The authors declare no competing financial interests.

Data Availability: The data that support the findings of this study are available from the corresponding author upon reasonable request.

Supporting Information: Additional measurements on the bilayer $CrCl_3$ MTJ and modelling of the tunneling current; Characterization and discussion of the magnetic properties of multilayer and monolayer $CrCl_3$; PL measurement on monolayer $CrCl_3$.

REFERENCES

1. Huang, B., Clark, G., Navarro-Moratalla, E., Klein, D.R., Cheng, R., Seyler, K.L., Zhong, D., Schmidgall, E., McGuire, M.A., Cobden, D.H. et al. Layer-dependent ferromagnetism in a van der Waals crystal down to the monolayer limit. *Nature* **546**, 270-273 (2017).
2. Gong, C., Li, L., Li, Z., Ji, H., Stern, A., Xia, Y., Cao, T., Bao, W., Wang, C., Wang, Y. et al. Discovery of intrinsic ferromagnetism in two-dimensional van der Waals crystals. *Nature* **546**, 265-269 (2017).
3. Ghazaryan, D., Greenaway, M.T., Wang, Z., Guarochico-Moreira, V.H., Vera-Marun, I.J., Yin, J., Liao, Y., Morozov, S.V., Kristanovski, O., Lichtenstein, A.I. et al. Magnon-assisted tunnelling in van der Waals heterostructures based on $CrBr_3$. *Nature Electronics* **1**, 344-349 (2018).
4. Lin, M.-W., Zhuang, H.L., Yan, J., Ward, T.Z., Puretzky, A.A., Rouleau, C.M., Gai, Z., Liang, L., Meunier, V., Sumpter, B.G. et al. Ultrathin nanosheets of $CrSiTe_3$: a semiconducting two-dimensional ferromagnetic material. *Journal of Materials Chemistry C* **4**, 315-322 (2016).
5. Yao, T., Mason, J.G., Huiwen, J., Cava, R.J. & Kenneth, S.B. Magneto-elastic coupling in a potential ferromagnetic 2D atomic crystal. *2D Materials* **3**, 025035 (2016).
6. McGuire, M.A., Dixit, H., Cooper, V.R. & Sales, B.C. Coupling of Crystal Structure and Magnetism in the Layered, Ferromagnetic Insulator CrI_3. *Chemistry of Materials* **27**, 612-620 (2015).

7. Bonilla, M., Kolekar, S., Ma, Y., Diaz, H., Kalappattil, V., Das, R., Eggers, T., Gutierrez, H.R., Phan, M.-H. & Batzill, M. Strong room-temperature ferromagnetism in VSe_2 monolayers on van der Waals substrates. *Nature Nanotechnology* **13**, 289-293 (2018).
8. Tan, C., Lee, J., Jung, S.-G., Park, T., Albarakati, S., Partridge, J., Field, M.R., McCulloch, D.G., Wang, L. & Lee, G. Hard magnetic properties in nanoflake van der Waals Fe_3GeTe_2. *Nature Communications* **9**, 1554 (2018).
9. Novoselov, K.S., Mishchenko, A., Carvalho, A. & Castro Neto, A.H. 2D materials and van der Waals heterostructures. *Science* **353**, aac9439 (2016).
10. Yuasa, S., Nagahama, T., Fukushima, A., Suzuki, Y. & Ando, K. Giant room-temperature magnetoresistance in single-crystal Fe/MgO/Fe magnetic tunnel junctions. *Nature Materials* **3**, 868 (2004).
11. Lee, G.-H., Yu, Y.-J., Lee, C., Dean, C., Shepard, K.L., Kim, P. & Hone, J. Electron tunneling through atomically flat and ultrathin hexagonal boron nitride. *Applied Physics Letters* **99**, 243114 (2011).
12. Britnell, L., Gorbachev, R.V., Jalil, R., Belle, B.D., Schedin, F., Mishchenko, A., Georgiou, T., Katsnelson, M.I., Eaves, L., Morozov, S.V. et al. Field-Effect Tunneling Transistor Based on Vertical Graphene Heterostructures. *Science* **335**, 947-950 (2012).
13. Song, T., Cai, X., Tu, M. W.-Y., Zhang, X., Huang, B., Wilson, N.P., Seyler, K.L., Zhu, L., Taniguchi, T., Watanabe, K. et al. Giant tunneling magnetoresistance in spin-filter van der Waals heterostructures. *Science* **6394**, 1214-1218 (2018).
14. Klein, D.R., MacNeill, D., Lado, J.L., Soriano, D., Navarro-Moratalla, E., Watanabe, K., Taniguchi, T., Manni, S., Canfield, P., Fernandez-Rossier, J. et al. Probing magnetism in 2D van der Waals crystalline insulators via electron tunneling. *Science* **6394**, 1218-1222 (2018).
15. Zhong, D., Seyler, K.L., Linpeng, X., Cheng, R., Sivadas, N., Huang, B., Schmidgall, E., Taniguchi, T., Watanabe, K., McGuire, M.A. et al. Van der Waals engineering of ferromagnetic semiconductor heterostructures for spin and valleytronics. *Science Advances* **3**, e1603113 (2017).
16. Jiang, S., Li, L., Wang, Z., Mak, K.F. & Shan, J. Controlling magnetism in 2D CrI_3 by electrostatic doping. *Nature Nanotechnology* **13**, 549-553 (2018).
17. Wang, Z., Sapkota, D., Taniguchi, T., Watanabe, K., Mandrus, D. & Morpurgo, A.F. Tunneling Spin Valves Based on Fe_3GeTe_2/hBN/Fe_3GeTe_2 van der Waals Heterostructures. *Nano Letters* **18**, 4303-4308 (2018).
18. Ralph, D.C. & Stiles, M.D. Spin transfer torques. *Journal of Magnetism and Magnetic Materials* **320**, 1190-1216 (2008).
19. Lee, J.-U., Lee, S., Ryoo, J.H., Kang, S., Kim, T.Y., Kim, P., Park, C.-H., Park, J.-G. & Cheong, H. Ising-Type Magnetic Ordering in Atomically Thin $FePS_3$. *Nano Letters* **16**, 7433-7438 (2016).
20. Fei, Z., Huang, B., Malinowski, P., Wang, W., Song, T., Sanchez, J., Yao, W., Xiao, D., Zhu, X., May, A.F. et al. Two-dimensional itinerant ferromagnetism in atomically thin Fe_3GeTe_2. *Nature Materials* **17**, 778-782 (2018).
21. Deng, Y., Yu, Y., Song, Y., Zhang, J., Wang, N.Z., Sun, Z., Yi, Y., Wu, Y.Z., Wu, S., Zhu, J. et al. Gate-tunable room-temperature ferromagnetism in two-dimensional Fe_3GeTe_2. *Nature* **563**, 94-99 (2018).
22. Narath, A. Low-Temperature Sublattice Magnetization Of Antiferromagnetic $CrCl_3$. *Physical Review* **131**, 1929-1942 (1963).
23. Narath, A. & Davis, H.L. Spin-Wave Analysis of the Sublattice Magnetization Behavior of Antiferromagnetic and Ferromagnetic $CrCl_3$. *Physical Review* **137**, A163-A178 (1965).
24. Kuhlow, B. Magnetic Ordering in $CrCl_3$ at the Phase Transition. P*hysica Status Solidi (a)* **72**, 161-168 (1982).

25. McGuire, M.A., Clark, G., KC, S., Chance, W.M., Jellison, G.E., Cooper, V.R., Xu, X. & Sales, B.C. Magnetic behavior and spin-lattice coupling in cleavable van der Waals layered $CrCl_3$ crystals. *Physical Review Materials* **1**, 014001 (2017).
26. de Jongh, L.J. & Miedema, A.R. Experiments on simple magnetic model systems. *Advances in Physics* **23**, 1-260 (1974).
27. Mondal, M., Kumar, S., Chand, M., Kamlapure, A., Saraswat, G., Seibold, G., Benfatto, L. & Raychaudhuri, P. Role of the Vortex-Core Energy on the Berezinskii-Kosterlitz-Thouless Transition in Thin Films of NbN. *Physical Review Letters* **107**, 217003 (2011).
28. Kosterlitz, J.M. & Thouless, D.J. Ordering, metastability and phase transitions in two-dimensional systems. *Journal of Physics C: Solid State Physics* **6**, 1181 (1973).
29. Hao, X., Moodera, J.S. & Meservey, R. Thin-film superconductor in an exchange field. *Physical Review Letters* **67**, 1342-1345 (1991).
30. Katmis, F., Lauter, V., Nogueira, F.S., Assaf, B.A., Jamer, M.E., Wei, P., Satpati, B., Freeland, J.W., Eremin, I., Heiman, D. et al. A high-temperature ferromagnetic topological insulating phase by proximity coupling. *Nature* **533**, 513-516 (2016).
31. Liu, X., Hsu, H.-C. & Liu, C.-X. In-Plane Magnetization-Induced Quantum Anomalous Hall Effect. *Physical Review Letters* **111**, 086802 (2013).
32. Miron, I.M., Garello, K., Gaudin, G., Zermatten, P.-J., Costache, M.V., Auffret, S., Bandiera, S. Rodmacq, B., Schuhl, A. & Gambardella, P. Perpendicular switching of a single ferromagnetic layer induced by in-plane current injection. *Nature* **476**, 189-193 (2011).
33. Pai, C.-F., Liu. L., Li, Y., Tseng, H.W., Ralph, D.C. & Buhrman, R.A. Spin transfer torque devices utilizing the giant spin Hall effect of tungsten. *Applied Physics Letters* **101**, 122404 (2012).
34. Seyler, K.L., Zhong, D., Klein, D.R., Gao, S., Zhang, X., Huang, B., Navarro-Moratalla, E., Yang, L., Cobden, D.H., McGuire, M.A. et al. Ligand-field helical luminescence in a 2D ferromagnetic insulator. *Nature Physics* **14**, 277-281 (2018).
35. Miao, G.-X., Müller, M. & Moodera, J.S. Magnetoresistance in Double Spin Filter Tunnel Junctions with Nonmagnetic Electrodes and its Unconventional Bias Dependence. *Physical Review Letters* **102**, 076601 (2009).
36. Wei, P., Lee, S., Lemaitre, F., Pinel, L., Cutaia, D., Cha, W., Katmis, F. Zhu, Y., Heiman, D., Hone, J. et al. Strong interfacial exchange field in the graphene/EuS heterostructure. *Nature Materials* **15**, 711-716 (2016).
37. Klein, D.R., MacNeill, D., Song, Q., Larson, D.T., Fang, S., Xu, M., Ribeiro, R.A., Canfield, P.C., Kaxiras, E., Comin, R. et al. Giant enhancement of interlayer exchange in an ultrathin 2D magnet. *eprint arXiv:1903.00002*, arXiv:1903.00002 (2019).
38. Kim, H.H., Yang, B., Li, S., Jiang, S., Jin, C., Tao, Z., Nichols, G., Sfigakis, F., Zhong, S., Li., C. et al. Evolution of interlayer and intralayer magnetism in three atomically thin chromium trihalides. *eprint arXiv:1903.01409*, arXiv:1903.01409 (2019).
39. Wang, L., Meric, I., Huang, P.Y., Gao, Q., Gao, Y., Tran, H., Taniguchi, T., Watanabe, K., Campos, L.M., Muller, D.A. et al. One-Dimensional Electrical Contact to a Two-Dimensional Material. *Science* **342**, 614-617 (2013).